Phys. Status Solidi A **211,** No. 2, 449–454 (2014) / **DOI** 10.1002/pssa.201300497

physica status solidi a
www.pss-a.com
applications and materials science

Investigation of the factors influencing nanostructure array growth by PLD towards reproducible wafer-scale growth

Vinod E. Sandana*[,1], David. J. Rogers[1], Féréchteh Hosseini Teherani[1], Philippe Bove[1], and Manijeh Razeghi[2]

[1] Nanovation, 8 Route de Chevreuse, 78117 Châteaufort, France
[2] Center for Quantum Devices, ECE Department, Northwestern University, Evanston, IL 60208, USA

Received 10 August 2013, revised 11 August 2013, accepted 11 December 2013
Published online 15 January 2014

Keywords catalyst-free, nanostructure, wide area, ZnO

* Corresponding author: e-mail vinodsandana@aol.fr, Phone: +33 6 25 47 31 32, Fax: +33 9 51 26 88 56

The growth of catalyst-free ZnO nanostructure arrays on silicon (111) substrates by pulsed laser deposition was investigated. Without an underlayer, randomly oriented, micron-scale structures were obtained. Introduction of a *c*-axis oriented ZnO underlayer resulted in denser arrays of vertically oriented nanostructures with either tapering, vertical-walled or broadening forms, depending on background Ar pressure. Nanostructure pitch seemed to be determined by underlayer grain size while nanostructure widths could be narrowed from ~100–500 to ~10–50 nm by a 50 °C increase in growth temperature. A dimpled underlayer topography correlated with the moth-eye type arrays while a more granular surface was linked to vertically walled nanocolumns. Between-wafer reproducibility was demonstrated for both moth-eye and vertical nanocolumn arrays. Broadening nanostructures proved difficult to replicate, however. Full 2 inch wafer coverage was obtained by rastering the target with the laser beam.

1 Introduction ZnO is a direct wide bandgap semiconductor ($E_g \sim 3.4$ eV) with intrinsically high transparency over the whole visible range and a resistivity that can be tuned from semi-insulating right through to semi-metallic by doping [1–3]. Pulsed laser deposition (PLD) is often adopted for the growth of ZnO because of the high quality thin films and nanostructures that can be produced [4–11]. In previous papers, it was demonstrated that PLD can also give catalyst-free, self-forming and vertically-aligned ZnO nanostructure arrays with excellent crystallinity and optical quality [12].

This research has the dual aims of developing better understanding of the mechanism by which such nanostructures form and of making them in a controlled, reproducible manner on the wafer scale (2 inch diameter wafers).

2 Experiment Self-forming, catalyst-free ZnO nanostructure arrays were grown on Si (111) substrates by PLD from a 99.99% pure sintered ZnO using a KrF excimer laser (248 nm), as described elsewhere [13–15]. Si substrates were chosen because they were found to give excellent results in previous studies [16, 17]. In order to combat the inhomogeneous nature of the PLD plasma, nanostructure growth was extended over 2 inch wafers via the installation of an optical scanning system for the incident laser beam which rastered the spot over the target. The sample morphology was studied using a Hitachi S4800 field emission-scanning electron microscope (SEM). Other characterization data, including X-ray diffraction and photoluminescense were reported elsewhere [13–15].

3 Results and discussion

3.1 Obtaining vertically-oriented, catalyst-free nanostructure arrays Growth temperature (T_s) and Ar partial pressure (P_{Ar}) were found to be key parameters for the realization of nanostructures. For growth directly on the substrate, randomly oriented nanostructures (up to micron scale in width) were obtained, as illustrated in Fig. 1.

Vertically-aligned nanostructure arrays could be obtained by introducing a *c*-axis oriented ZnO thin film underlayer. This was achieved by growing initially in thin film mode (lower temperature) then switching to nanostructure growth mode (higher temperature). Three main

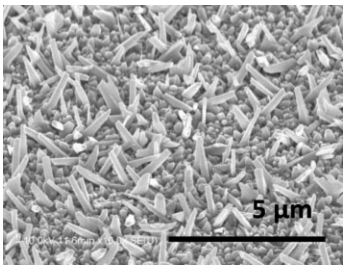

Figure 1 SEM image of disordered ZnO nanostructures grown without a buffer layer.

types of self-forming ZnO nanostructure arrays were observed: vertical, tapering, and broadening (as shown in Fig. 2).

The prerequisite of a *c*-axis oriented ZnO underlayer for obtaining vertically-aligned array is consistent with the crystallographic orientation of the underlayer determining the physical orientation of the nanowire (as was found for chemical growth of nanowires on PLD-grown thin film templates [18]).

Figure 3 (photograph and SEM images) shows a sharp transition in appearance between an area with vertically aligned ZnO nanostructures (darker appearance) and an area with larger, disoriented, ZnO microrods (silvery appearance).

Indeed, the vertically oriented arrays were confirmed, elsewhere [19], to have excellent anti-reflection properties, which predispose them for use in optical applications, such as solar cells and sensors (anti-reflection and light trapping layers) [19–23] and LEDs (extraction) [24, 25]. It is not clear whether it is the preferred vertical alignment, more regular form, higher density or finer scale (sub-optical), which underlies the improved anti-reflection properties.

In previous studies, it was also found that vertically oriented ZnO nanostructure arrays could be grown on various substrates (Si (111), *c*-Al_2O_3, ZnO, and steel). It was observed that (for the same growth conditions) the width, pitch, crystallographic quality, crystallographic orientation and optical quality depended strongly on the kind of substrate that was adopted. This is probably due to variation in grain size and crystallographic orientation in the

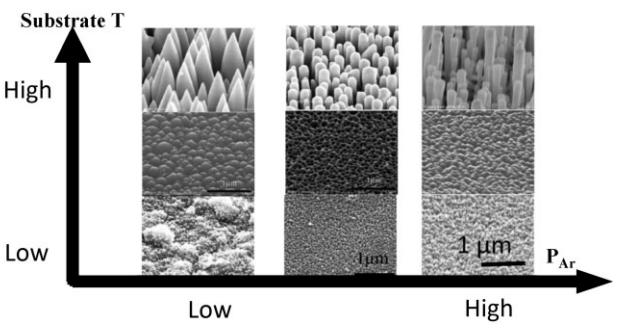

Figure 2 SEM images illustrating ZnO nanostructure morphology variation with growth temperature and Ar partial pressure.

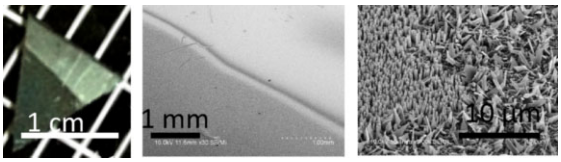

Figure 3 Photograph and SEM images showing the distinct difference in reflection between (darker) vertically aligned ZnO nanostructures (on a ZnO underlayer) and (lighter) disoriented nanostructures (grown directly on Si).

underlayer grown on different substrates, the influence of which is confirmed by Fig. 4.

3.2 Between-wafer reproducibility SEM study of six different wafers with moth-eye-type arrays showed that although there were some slight variations between samples in terms of width, pitch, height-homogeneity and tip angle, all the nanocones show a preferred vertical orientation and a conical structure with widths in the 100–500 nm range and pitch in the 400–1000 nm range. There was also no evidence of sample fragility in terms of fractured/damaged nanostructures.

As for the moth-eye arrays, SEM study of six different wafers with vertical-walled nanocolumn arrays, revealed relatively little variation between samples in terms of width, pitch, orientation, height-homogeneity and tip angle. All the nanocolumns showed a preferred vertical orientation with widths in the 100–500 nm range and pitch in the 400–800 nm range (packing seems denser than for the nanocones). There is also no evidence of sample fragility in terms of fractured/damaged nanostructures.

The broadening nanostructure arrays (see Introduction), however, proved less ordered and more difficult to reproduce.

3.3 Development of the different nanostructure array forms The SEM images in Fig. 5 show two distinctive kinds of underlayer morphologies that were commonly observed.

The mottled underlayer morphology (on the left) was found to be associated with the moth-eye nanocone arrays while the more granular surface (right hand side) was

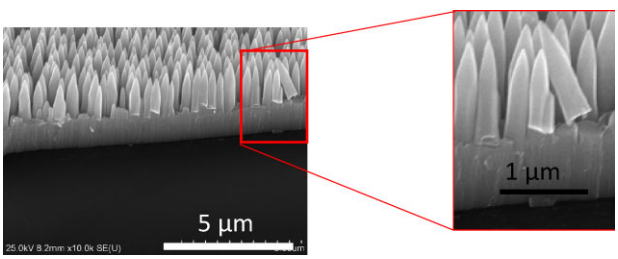

Figure 4 SEM sectional images showing how the grains in the ZnO underlayer determine the width, pitch and orientation of the nanostructures (the hexagonal underlayer grain can be discerned in the zoom on the fracture interface of a broken nanocone).

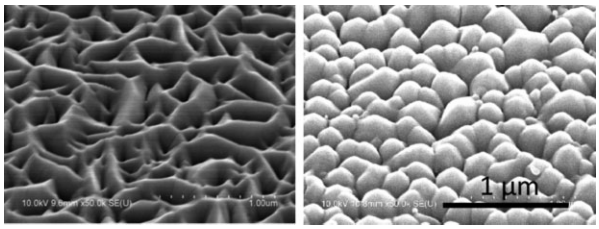

Figure 5 SEM images of the two distinctive kinds of underlayer morphologies that were most commonly observed (same scale bar for both images).

correlated with columnar nanoarrays (see evidence in Fig. 12).

For the mottled underlayer, further SEM investigations revealed that the hollows/indentations bottom out into a kind of dimple. The SEM image below (Fig. 6) shows that the structure is actually faceted and thus the surface morphology appears to be the result of crystallinity of the buffer layer.

In the sectional SEM images (Fig. 6), we can directly see how both the dimpled and granular morphologies are the result of the underlying crystal grain structure in the buffer layer.

Indeed, grain boundaries can be discerned in the left SEM image in Fig. 5, which reveals that the ridge-like features of the dimpled morphology appear to be coalescing links between the peaks of neighboring grains.

This link of nanostructure form with underlayer topography does not explain why different forms of nanostructures occur, however. Indeed, Laudies and Ballman [26] found that for equilibrium growth of bulk wurtzite ZnO crystals, the [0001] growth rate is ∼2× faster than that for [10–10] and that the [10–11] growth rate is intermediate, which should lead to a crystal of the form shown in Fig. 7.

This would not explain the formation of the conical (moth-eye) nanostructure with smooth (non-faceted) sidewalls, however. A possible explanation for such a form was evoked by Wang et al. [27], who proposed that the adatoms arriving at the growth front are not all chemisorbed and some leave the surface to subsequently renucleate in clusters on the (0001) surface. These clusters eventually form a cone (see illustration in Fig. 8).

In a first instance, isolated nanostructures were found in some samples that seemed coherent with this hypothesis, as shown in Fig. 9.

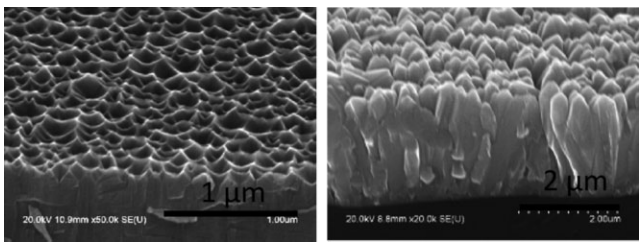

Figure 6 Sectional SEM images of mottled/dimpled and granular morphologies ZnO buffer underlayer.

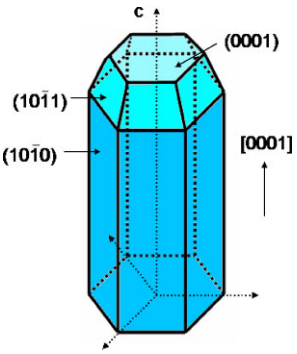

Figure 7 Illustration of the equilibrium ZnO wurtzite crystal.

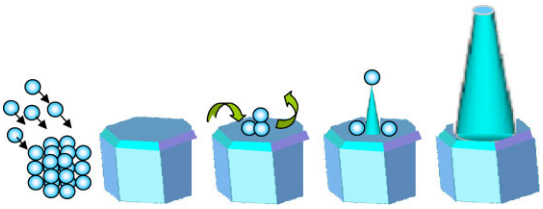

Figure 8 Illustration of a model for the formation of conical moth-eye nanostructures. The first stage represents the adatom arriving at the growth front. The third stage represents the renucleation of adatom which are not chemisorbed (after Wang et al. [27]).

Analysis of the nanostructure array development, however, led us to believe that this was not the growth mechanism of the moth-eye nanostructure arrays. The inclined-angle SEM images, Fig. 10, show various development stages of a moth-eye type nanostructure array.

From these images, it would appear that nanostructure growth originates from an amplified roughness of the underlayer morphology rather than a redeposition/renucleation centred on a nanocolumn.

The SEM image of longer nanocones in Fig. 11 shows that the sidewalls eventually become more vertically oriented during growth with the maximum width/pitch of the nanocones constrained by the grain size in the underlayer.

Thus, it would appear that a fine conical nanostructure develops at a tip that emerges in the surface morphology and widens until it is limited by the underlying grain and/or the

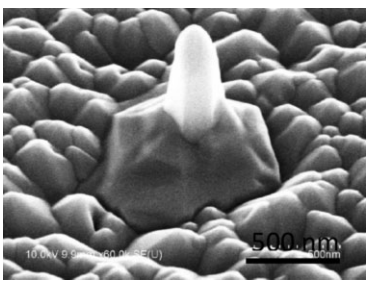

Figure 9 SEM image of a ZnO nanostructure consistent with the results of Wang et al. [27] growth mechanism hypothesis.

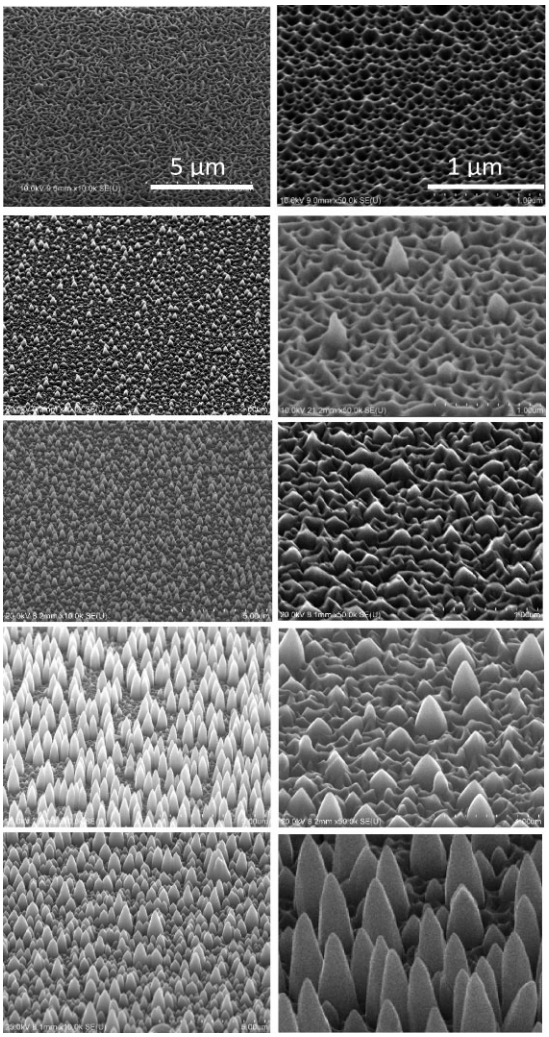

Figure 10 SEM images of the various development stages of a moth-eye type ZnO nanostructure array (the scale bar for the images on the left is 5 μm while that for those on the right is 1 μm).

neighboring nanocone. At this point, the sidewalls become more vertical. The slope of the tip, however, remains as it was in the initial nanotip nucleus, which is a higher angle than would have been expected based on the studies of Laudies et al. [26] of equilibrium bulk ZnO crystal

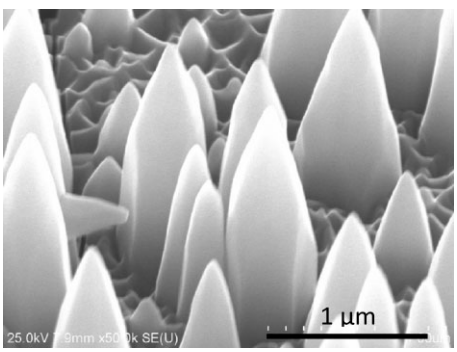

Figure 11 SEM images of longer ZnO nanocones.

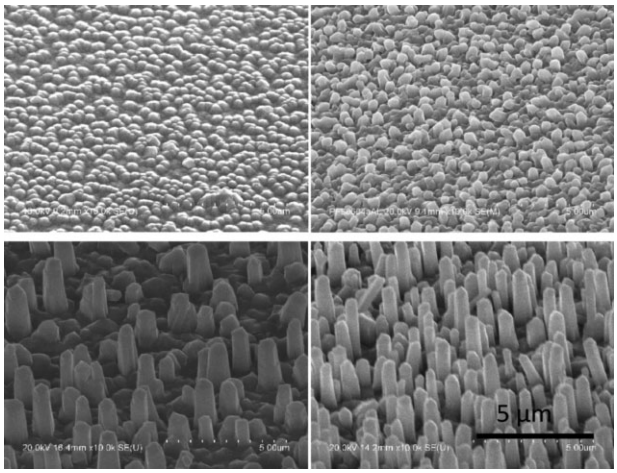

Figure 12 Inclined-angle SEM images showing the development stages for a columnar nanostructure array (same scale bar for all images).

growth. This situation could well be a result of the PLD deposition approach/conditions, which produce an externally dictated growth rate (based on a pulsed adatom supply) and a resultant freezing-in of structures which may not have reached thermodynamic equilibrium (due to, for instance, insufficient surface mobility and/or the arrival of the next wave of adatoms before surface diffusion allows them to reach a configuration that minimizes surface free energy).

Figure 12 shows development stages for a columnar nanostructure array. The images are consistent with the columnar growth being a continuation of the granularity of the underlayer with the density of the nanocolumns being determined by the grain size in the underlayer.

Hence, we were able to establish a correlation between underlayer surface morphology and the faceting/form of both the moth-eye nanocones and the vertically walled nanocolumns.

With regards to the smooth surfaces observed for some nanostructures, further examination revealed that all the nanostructure arrays were, in fact, hexagonally faceted but this was not always visible due to the imaging conditions used in the SEM (see Fig. 13).

It can be seen that for a 25 keV accelerating voltage (left hand image) the nanostructures appear rounded whereas, for a 2 keV accelerating voltage (right hand image), hexagonal faceting is apparent. This is because a higher accelerating voltage induces surface transparency in the

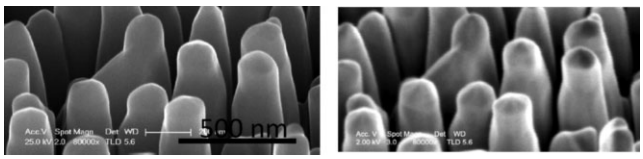

Figure 13 SEM images of ZnO nanocolumns at different accelerating voltages.

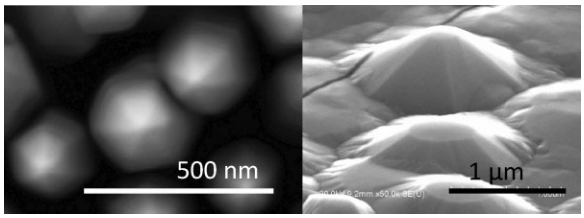

Figure 14 On the left is a top-view SEM image of moth-eye type nanostructures. On the right is an SEM image showing varying kinds of faceting (more peaked and flat-topped).

image. Hexagonal faceting was also present for the moth-eye type nanostructures, as can be seen in Fig. 14.

Thus, the apparent smooth surface appears to be an artifact of the SEM imaging conditions and the nanocolumn arrays actually present tips with facet angles which are coherent with Landies' equilibrium crystal.

This does not resolve all the questions with regard to faceting, however, since the nanocones and nanocolumns mostly exhibit a peaked tip instead of flat tops. We investigated this difference but could not confirm the hypothesis of there being a direct cause/effect relationship with certain growth conditions. Indeed, the SEM image in Fig. 14 shows that different kinds of faceting (more peaked and more flat-topped) can be obtained under the same growth conditions.

3.4 Realisation of finer nanostructure arrays

Growth parameter space was further explored in order to find how to better control the nanostructures. The main new finding was that slight further elevation of growth temperature (+∼50 °C) produced much finer vertically oriented "nanoneedles". The SEM images in Fig. 15 illustrate this.

The nanostructure arrays have widths and pitches of ∼10–50 nm. Although these nanoneedles are an order of magnitude narrower than the prior nanostructures (see Fig. 2), the pitch (100–500 nm) is similar. This indicates that the nucleation density was comparable, in spite of the difference in the growth parameters during nucleation/growth, and is consistent with a dependence of nucleation density on the underlayer.

Although the larger moth-eye and nanocolumn structures might be more adapted for anti-reflection, detector/sensor and light extraction applications, these finer nanoneedles could be more amenable to other applications, such as one where a filler would be required (e.g. n-ZnO/p-polymer heterojunctions) or quantum dot sensitised solar cells.

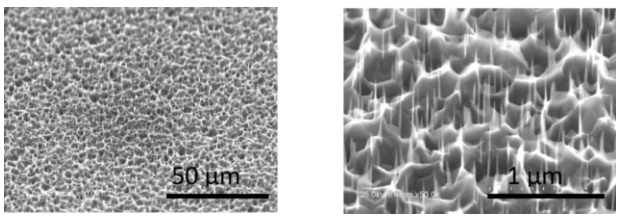

Figure 15 SEM images of nanostructure arrays having widths and pitches of about 10–50 nm and 100–500 nm, respectively.

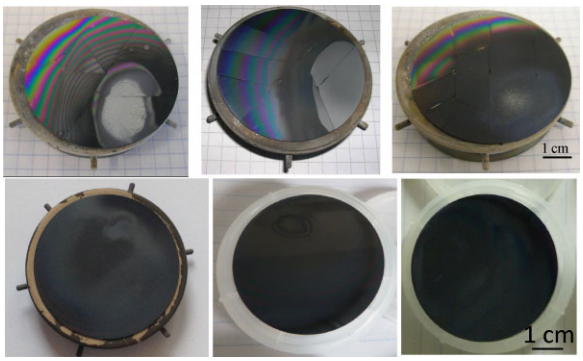

Figure 16 The three upper images show PLD-grown nanostructures on 2 inch diameter Si wafers without the use of optical rastering (N.B. wafers were deliberately cleaved before PLD in order to reduce the need to manipulate the sample after growth). The three lower images show PLD-grown nanostructures on 2 inch diameter Si wafers with optical scanning of the laser beam.

An interesting corollary of this finding is the general observation that the nanostructure form exhibits a very strong temperature dependence at higher temperatures. Thus, some of the issues with in-wafer homogeneity may originate from slight temperature variations across the substrate rather than problems with the optical scanning.

3.5 Reproducible growth of nanostructure arrays

The three upper images in Fig. 16 show the result of typical PLD nanostructure growth on a Si wafer without optical rastering of the laser beam. Darker regions are where vertically aligned nanostructure arrays have formed.

The wafers show poor within-wafer and between-wafer homogeneity due to the inhomogeneous nature of the PLD plasma plume.

The lower row of photographs in Fig. 16 illustrates the impact of the optical scanning system on three ZnO nanostructure growth runs for 2 inch diameter Si wafers.

The wafers now have full coverage and much better within-wafer and between-wafer reproducibility and homogeneity.

4 Conclusions

This work was focused on developing and understanding of the factors influencing the form, orientation, size, and spacing of catalyst-free, self-forming nanostructure arrays grown by PLD in order to obtain controlled/reproducible growth on the wafer scale. This was done by investigating the impact of the underlayer, varying the SEM imaging conditions, exploring the effect of further increasing growth temperature, studying the nanostructure development with growth time and introducing optical rastering of the plasma plume.

Vertically aligned nanostructure arrays proved relatively reproducible in terms of form (moth-eye and columnar

types), width (~100/500 nm) and pitch (~400/1000 nm). Full 2 inch wafer coverage was achieved but some problems of in-wafer homogeneity remain in spite of varying the rastering algorithm. This is most probably due to temperature fluctuations across the substrate combined with a high sensitivity of nanostructure form to growth temperature at elevated temperatures.

The smooth/rounded appearance of the nanostructure tips was found to be an illusion due to the relatively high accelerating voltage used in some SEM studies. Nanostructures were seen to form whether or not an underlayer was present but the presence of a *c*-axis oriented ZnO underlayer was a prerequisite for vertically aligned arrays.

A mottled/dimpled underlayer surface morphology seemed to be associated with moth-eye growth while a more granular topology correlated with columnar nanostructure arrays. The nucleation density and pitch/density of the nanostructures appeared to be constrained by the grain size in the underlayer.

A slight increase in growth temperature (+~50 °C) was observed to produce much finer vertically oriented nanoneedles with widths of about 10–50 nm. The pitch remained at the same scale as for the other nanostructure arrays, however. Insight into the development of the nanostructure form/properties was obtained by analyzing the evolution during growth. It was deduced that the nanoarrays seem to originate as fine tips at the underlayer surface and that the sidewalls eventually become more vertically oriented when the lateral growth is constrained by the grain size in the underlayer.

Acknowledgements The authors would like to thank the US Army for funding this work.

References

[1] D. C. Look, in: Zinc Oxide: A Material for Micro- and Optoelectronic Applications, edited by N. H. Nickel, NATO Science Ser. II: Mathematics, Physics and Chemistry Vol. 194 (Springer, Netherland, 2005), p. 37.
[2] D. J. Rogers and F. Hosseini Teherani, Encyclopedia of Materials: Science and Technology (Elsevier, Oxford, 2010), pp. 1–5.
[3] D. J. Rogers, F. Hosseini Teherani, V. E. Sandana, and M. Razeghi, Proc. SPIE **7605**, 76050K-1 (2010).
[4] V. Gupta, P. Bhattacharya, Yu. I. Yuzuk, K. Sreenivas, and R. S. Katiyar, J. Cryst. Growth **287**, 39 (2006).
[5] S. J. Henley, M. N. R. Ashfold, D. P. Nicholls, P. Wheatley, and D. Cherns, Appl. Phys. A **79**, 1169 (2004).
[6] E. M. Kaidashev, M. Lorenz, A. Rahm, H. C. Semmelhack, and M. Grundmann, Appl. Phys Lett. **82**, 6951 (2003).
[7] J. H. Kim, K. A. Jeon, H. S. Kang, and S. Y. Lee, Superlattices Microstr. **39**, 60 (2006).
[8] M. Lorenz, E. M. Kaidashev, A. Rahm, T. Nobis, I. Lenzner, G. Wagner, D. Spemann, H. Hochmuth, and M. Grundmann, Appl. Phys. Lett. **86**, 143113 (2005).
[9] R. Nishimura, T. Sakano, T. Okato, T. Saiki, and M. Obara, Jpn. J. Appl. Phys. **47**, 4799 (2008).
[10] P. Gondoni, V. Russo, C. E. Bottani, A. L. Bassi, and C. S. Casari, MRS Proc. **1497**, (2013).
[11] A. Marcu, L. Trupina, R. Zamani, J. Arbiol, C. Grigoriu, and J. R. Morante, Thin Solid Films **14**, 4626 (2012).
[12] V. E. Sandana, D. J. Rogers, F. Hosseini Teherani, R. McClintock, C. Bayram, M. Razeghi, H.-J. Drouhin, M. C. Clochard, V. Sallet, G. Garry, and F. Falyouni, J. Vac. Sci. Technol. B **27**, 3 (2009).
[13] V. E. Sandana, D. J. Rogers,1 F. Hosseini Teherani, P. Bove, M. Molinari, M. Troyon, A. Largeteau, G. Demazeau, C. Scott, G. Orsal, H.-J. Drouhin, A. Ougazzaden, and M. Razeghi, Phys. Status Solidi C **10**, 1317 (2013).
[14] V. E. Sandana, D. J. Rogers, F. Hosseini Teherani, R. McClintock, M. Razeghi, H.-J. Drouhin, M. C. Clochard, V. Sallet, G. Garry, and F. Falyouni, Proc. SPIE **6895**, 68950Z (2008).
[15] D. J. Rogers, V. E. Sandana, F. Hosseini Teherani, M. Razeghi, and H.-J. Drouhin, Proc. SPIE **7217**, 721708-1 (2008).
[16] S. Harinipriya, B. Usmani, D. J. Rogers, V. E. Sandana, F. Hosseini Teherani, A. Lusson, P. Bove, H.-J. Drouhin, and M. Razeghi, Proc. SPIE **8263**, 82631Y1 (2012).
[17] J. L. Pau, J. Piqueras, D. J. Rogers, F. Hosseini Teherani, K. Minder, R. McClintock, and M. Razeghi, J. Appl. Phys. **107**, 033719 (2010).
[18] R. Erdeelyi, T. Nagata, D. J. Rogers, F. H. Teherani, Z. E. Horvath, Z. Labadi, Z. Baji, Y. Wakayama, and J. Volk, Cryst. Growth Des. **11**, 2515A (2011).
[19] M. Peres, V. E. Sandana, F. Teherani, and D. J. Rogers, Phys. Status Solidi A **247**(7), 1695 (2010).
[20] V. K. Narasimhan and Y. Cui, Nanophtonics **2**, 187 (2013).
[21] T. Soderstrom, D. Domine, A. Feltrin, M. Despeisse, F. Meillaud, G. Bugnon, M. Boccard, P. Cuony, F.-J. Haug, S. Fay, S. Nicolay, and C. Ballif, Proc. SPIE **7603**, 76030B (2010).
[22] L. Tsakalakos, Mater. Sci. Eng. R **62**, 175 (2008).
[23] D. J. Rogers, V. E. Sandana, F. Hosseini Teherani, S. Gautier, G. Orsal, T. Moudakir, M. Molinari, M. Troyon, M. Peres, M. Soares, A. Neves, T. Monteiro, D. McGrouther, J. Chapman, H.-J. Drouhin, M. Razeghi, and A. Ougazzaden, Renew. Energy Environ. OSA PWB3 (2011).
[24] J. Zhong, H. Chen, G. Saraf, Y. Lu, C. K. Choi, J. J. Song, D. M. Mackie, and H. Shen, Appl. Phys. Lett. **90**, 203515 (2007).
[25] D. J. Rogers, F. Hosseini Teherani, P. Bove, R. McClintock, and M. Razeghi, SPIE Newsroom. 15 June 2012, http://spie.org/x87495.xml?pf=true&ArticleID=x87495.
[26] R. A. Laudies and A. A. Ballman, J. Phys. Chem. **64**, 688 (1960).
[27] G. Z. Wang, Y. Wang, M. Y. Yau, C. Y. To, C. J. Deng, and D. H. L. Ng, Mater. Lett. **59**, 3870 (2005).

